AGU ADVANCING EARTH AND SPACE SCIENCE

JGR Biogeosciences

RESEARCH ARTICLE
10.1029/2022JG007132

Key Points:

- Porewater profiles in Subterranean estuaries (STEs) vary across space and time
- Denitrification within STEs can significantly reduce nutrient loading via submarine groundwater discharge (SGD)
- Nutrient fluxes via SGD were of the same magnitude as diffusive benthic nutrient fluxes, but lower than fluvial inputs

Supporting Information:

Supporting Information may be found in the online version of this article.

Correspondence to:

S. J. Wilson,
wilsonsj@si.edu

Citation:

Wilson, S. J., Anderson, I. C., Song, B., & Tobias, C. R. (2023). Temporal and spatial variations in subterranean estuary geochemical gradients and nutrient cycling rates: Impacts on groundwater nutrient export to estuaries. *Journal of Geophysical Research: Biogeosciences*, *128*, e2022JG007132. https://doi.org/10.1029/2022JG007132

Received 10 AUG 2022
Accepted 13 APR 2023

Author Contributions:

Conceptualization: Stephanie J. Wilson, Iris C. Anderson, Bongkeun Song, Craig R. Tobias
Data curation: Stephanie J. Wilson
Formal analysis: Stephanie J. Wilson
Funding acquisition: Iris C. Anderson, Bongkeun Song, Craig R. Tobias
Investigation: Stephanie J. Wilson, Bongkeun Song
Methodology: Iris C. Anderson, Bongkeun Song, Craig R. Tobias
Project Administration: Bongkeun Song
Supervision: Iris C. Anderson, Bongkeun Song, Craig R. Tobias
Writing – original draft: Stephanie J. Wilson
Writing – review & editing: Iris C. Anderson, Bongkeun Song, Craig R. Tobias

Temporal and Spatial Variations in Subterranean Estuary Geochemical Gradients and Nutrient Cycling Rates: Impacts on Groundwater Nutrient Export to Estuaries

Stephanie J. Wilson[1,2], Iris C. Anderson[1], Bongkeun Song[1], and Craig R. Tobias[3]

[1]Virginia Institute of Marine Science, William & Mary, Gloucester Point, VA, USA, [2]Smithsonian Environmental Research Center, Edgewater, MD, USA, [3]Department of Marine Sciences, UConn Avery Point, Groton, CT, USA

Abstract Subterranean estuaries (STEs) form at the land-sea boundary where groundwater and seawater mix. These biogeochemically reactive zones influence groundwater-borne nutrient concentrations and speciation prior to export via submarine groundwater discharge (SGD). We examined a STE located along the York River Estuary (YRE) to determine if SGD delivers dissolved inorganic nitrogen (DIN) and phosphorus (DIP) to the overlying water. We assessed variations in STE geochemical profiles with depth across locations, times, and tidal stages, estimated N removal along the STE flow path, measured hydraulic gradients to estimate SGD, and calculated potential nutrient fluxes. Salinity, dissolved oxygen (DO), DIN, and DIP varied significantly with depth and season ($p < 0.05$), but not location or tidal stage. Ammonium dominated the DIN pool deep in the STE. Moving toward the sediment surface, ammonium concentrations decreased as nitrate and DO concentrations increased, suggesting nitrification. Potential sediment N removal rates mediated by denitrification were <8 mmoles N m^{-2} d^{-1}. The total groundwater discharge rate was 38 ± 11 L m^{-2} d^{-1}; discharge followed tidal and seasonal patterns. Net SGD nutrient fluxes were 0.065–3.2 and 0.019–0.093 mmoles m^{-2} d^{-1} for DIN and DIP, respectively. However, microbial N removal in the STE may attenuate 0.58% to >100% of groundwater DIN. SGD fluxes were on the same order of magnitude as diffusive benthic fluxes but accounted for <10% of the nutrients delivered by fluvial advection in the YRE. Our results indicate the importance of STE biogeochemical transformations to SGD flux estimations and their role in coastal eutrophication and nutrient dynamics.

Plain Language Summary At the coastline, groundwater is released to coastal waters and at this land-sea boundary, groundwater and seawater meet and mix in subterranean estuaries (STEs). Groundwater can be a source of nutrients, trace metals, and carbon to the overlying water. Within the STE, groundwater-borne nutrients may be consumed or changed, altering what is released to overlying water. In this study, we examined a STE located in the Chesapeake Bay to characterize groundwater constituents with depth, measure nitrogen removal rates, and estimate groundwater nutrient export to coastal waters. Groundwater salinity, dissolved oxygen, and nutrients varied across space and time. Nitrogen removal was measured in sediment incubation experiments, revealing that sedimentary microbes in STEs can reduce some or all the nitrogen accumulated in groundwater. Groundwater discharge exported <10% of the nutrients flowing downstream in surface water and microbial nitrogen removal within the STE lowers nitrogen transport by groundwater. Our results highlight the importance of nutrient cycling in STEs and how these zones influence the role of groundwater as a nutrient source and, therefore, coastal water quality.

1. Introduction

Subterranean estuaries (STEs) form at the coastline where groundwater and seawater mix forming steep geochemical gradients (Moore, 1999). STEs, which are recognized as highly reactive zones for biogeochemical processing, influence the fate and transport of nutrients, organic matter, and trace metals discharged to the coastal ocean via groundwater (Duque et al., 2020; Moore, 1999, 2009; Santos et al., 2009, 2021). Seawater entering the STE is sulfate rich, typically oxic, and can provide labile dissolved organic matter (Slomp & Cappellen, 2004). In contrast, groundwater is generally anoxic, accumulates high levels of dissolved inorganic nitrogen (DIN) and phosphorus (DIP) from anthropogenic and natural sources along its flow path, and typically has recalcitrant organic matter and high concentrations of dissolved inorganic carbon (DIC) (Santos et al., 2021; Slomp &

Cappellen, 2004; Valiela et al., 1990). DIN concentrations in groundwater can be up to five times higher than the concentrations in surface waters (Slomp & Cappellen, 2004; Valiela et al., 1990).

Nitrogen (N) and phosphorus (P) are both limiting nutrients in marine systems and many coastal estuaries are N-limited (Nixon, 1995). There are several sources of N to coastal zones including drainage from the surrounding watersheds, rivers, surface water runoff, anthropogenic sources, and submarine groundwater discharge (SGD); however, of these sources SGD is the most poorly constrained (Leote et al., 2008; McKenzie et al., 2021; Moore, 2009). SGD can consist of meteoric groundwater or a mixture of meteoric groundwater and recirculated seawater that is discharged to overlying water (Boehm et al., 2006; Burnett et al., 2006; Slomp & Cappellen, 2004). SGD is distinct from diffusive benthic fluxes, which transport solutes across the sediment-water interface (Percuoco et al., 2015). Nutrient budgets for coastal zones often overlook SGD (Santos et al., 2021), which may be a considerable oversight as Cho et al. (2018) estimated that SGD discharges 2.3 ± 0.6 Tmol DIN yr^{-1} and 0.06 ± 0.02 Tmol DIP yr^{-1} to the global ocean, a flux on the same order of magnitude as that from rivers. SGD derived nutrients have also been shown to support primary production in a variety of coastal systems including oceanic islands (Kim et al., 2011), coastal embayments (Zhang et al., 2020), lagoons (Andrisoa et al., 2019), and estuaries (Guo et al., 2020). This is of particular concern for coastal regions already at risk for nutrient pollution and although measurements of groundwater nutrient inputs are becoming more common, they often remain unaccounted for in many regional nutrient budgets (Lake & Brush, 2015; Santos et al., 2021).

Microbial processes in STEs are important for determining the concentration and speciation of N in SGD, which may support potential phytoplankton blooms and further microbial N cycling upon discharge to receiving waters (Ruiz-González et al., 2021). Transformations within STEs have implications for N mobility in the subsurface, the fate of N after discharge, and influence the assemblage of primary producers present in overlying water. It is common, with a few exceptions (Kroeger & Charette, 2008), to ignore biogeochemical transformations that may attenuate or alter the species of N associated with SGD. Fluxes are commonly calculated as the product of the endmember concentration and a water flux with no attenuation or transformation along the flow path, assuming conservative transport of nutrients (Beck et al., 2016; Cho et al., 2018). This approach can result in biased estimations of nutrient export to coastal waters via SGD when nutrients are not transported conservatively. The effect of STE nutrient cycling and removal on SGD nutrient loading is not well characterized, but is critical to understanding the role of SGD derived nutrients in coastal biogeochemistry.

Processes including nitrification, denitrification, anaerobic ammonium oxidation (anammox), dissimilatory nitrate reduction to ammonia (DNRA), mineralization, and microbial N assimilation all influence the groundwater N pool. When oxygen is available in STEs, nitrification may oxidize ammonium (NH_4^+) to nitrate (NO_3^-) (Santoro et al., 2008; Schutte et al., 2017). Nitrification acts as a gateway to N removal processes such as denitrification and anammox (Brandes et al., 2007; Herbert, 1999), but also produces nitrous oxide (N_2O) as a byproduct. Denitrification is the enzymatically mediated stepwise reduction of NO_3^- to NO_2^-, NO, N_2O, and finally to N_2 gas. In anoxic STEs, denitrification has been reported, removing DIN that has accumulated in groundwater (Addy et al., 2002; Tobias et al., 2001; Wu et al., 2021). Anammox is the anaerobic oxidation of ammonium (NH_4^+) coupled to the reduction of NO_2^- to produce N_2. This process has been observed in both marine and freshwater environments (Lisa et al., 2014; Nicholls & Trimmer, 2009; Oshiki et al., 2016) and is important to N removal in some groundwater systems (Sáenz et al., 2012; Smith et al., 2015; Wu et al., 2021). DNRA may also occur in STEs, reducing NO_3^- to NH_4^+ and recycling DIN within the system (Wong et al., 2020). There are few rate measurements of N cycling processes in STEs, but they determine N fluxes via SGD. DIP cycling in STEs is usually dominated by abiotic processes, such as sorption to iron or manganese oxides (Charette & Sholkovitz, 2002; Spiteri, Slomp, Tuncay, & Meile, 2008; Spiteri, Cappellen, & Regnier, 2008) or co-precipitation with calcium carbonate (Cable et al., 2002). Sorption and precipitation immobilize DIP within the sediment, limiting its release in SGD, and increasing the N:P ratio of SGD. This was shown in a recent review by Santos et al. (2021) reporting that DIN:DIP ratios were higher than Redfield (16:1) in 75% of the 239 SGD studies compared.

In the face of widespread eutrophication, it is important to constrain fluxes of N and P in coastal zones. The potential for discharge of nutrients transported via SGD to coastal waters will vary over space and time due to the variation in temperature, groundwater discharge, nutrient concentrations, and cycling rates. Determining how nutrient cycling in STEs may modify inputs of N along the land-ocean continuum will further our understanding of coastal nutrient biogeochemistry. This is especially important in regions where excess nutrient inputs contribute to the formation of annual hypoxic zones and harmful algal blooms (HABs) (Anderson et al., 2002;

Mulholland et al., 2009; Reay, 2009). Often, nutrient inputs to coastal waters from river tributaries, runoff, and meteoric groundwater are estimated, but SGD (i.e., including fresh and saline groundwater) inputs remain largely unconstrained. Meteoric groundwater estimates only include the freshwater portion of groundwater that flows into the bay, whereas SGD is often a mixture of recirculated seawater and meteoric water formed in STEs. SGD has the potential to be a far larger source of nutrients than meteoric groundwater due to advection of porewater with high concentrations of DIN and DIP (Kroeger & Charette, 2008; Rodellas et al., 2018; Santos et al., 2021). The goal of this study was to examine the effects of variations in STE geochemistry and microbial N processing rates on potential nutrient discharge to the York River Estuary (YRE), a tributary of the Chesapeake Bay, and to determine the importance of SGD-derived nutrients when compared to other sources. We hypothesized that the STE is a significant source of nutrients to the overlying water compared to downriver and benthic fluxes. The specific objectives were to (a) characterize geochemical gradients in the STE with depth across location and time to determine the scales over which SGD should be quantified, (b) to measure potential N removal rates to assess the importance of microbial attenuation along the groundwater flowpath, and (c) to calculate potential fluxes to the overlying water and compare them to other sources of nutrients in the lower YRE.

2. Materials and Methods

2.1. Study Site Description

The Gloucester Point STE (GP-STE) is located near the mouth of the YRE in Virginia, USA (37.248884°N, 76.505324°W) (Figure 1a). The YRE, a microtidal and partially mixed tributary of the Chesapeake Bay, is roughly 52 km long from West Point (the confluence of the Pamunkey and Mattaponi rivers, YRE tributaries) to its mouth at Goodwin Island (Reay, 2009). Land use surrounding the YRE is primarily forested (61%) but is suburban adjacent to our study site (Reay, 2009). The temperate region surrounding the YRE typically experiences higher precipitation in the spring and summer months as compared to fall and winter. Precipitation data during the study period were retrieved from the NOAA National Estuarine Research Reserve System (NERRS) System-wide Monitoring Program meteorological site at Taskinas Creek along the YRE (2022, Figure S1 in Supporting Information S1). The Gloucester Point (GP) beach is a sandy sediment beach with a tidal range of ~0.8 m; it stretches about 20–30 m across and has man-made rock jetties at each end. A detailed site description of the GP-STE can be found in Beck et al. (2016).

2.2. Experimental Design

A network of dedicated piezometers (Charette et al., 2006) consisting of 2 cm screens (AMS Gas Vapor Tip) attached to FEP tubing (VersilOn, Saint-Gobain), was constructed at the GP-STE with depths ranging from 0 to 300 cm along the mid-tide line (MTL). Porewater and sediment were sampled to assess variability across location and time (Figure 1b). To examine seasonal variation in geochemical gradients and N process rates, STE porewater and sediment vibracores were collected in spring (9 April 2018), summer (9 July 2018), fall (2 October 2018), and winter (15 January 2019). To assess the variation throughout tidal cycles, porewater was sampled during two spring tides in the spring (7 May 2020) and summer (5 June 2020) at three tidal stages (low, mid, and high). Spatial variability in geochemical gradients was examined in three profiles, each three m apart, which were sampled once at low tide in spring 2020 (16 March 2020).

2.3. Seasonal Porewater Geochemical Monitoring

Porewater samples were collected at low tide during each season (spring, summer, fall, and winter) from piezometers placed at depths from 0 to 300 cm. The 17 piezometers sampled were 10, 20, 30, 40, 50, 60, 70, 80, 90, 100, 110, 120, 150, 175, 200, 250, and 300 cm deep and surface YRE water (denoted as 0 cm here) was also collected during seasonal sampling efforts. Masterflex C-Flex L/S Precision Pump tubing (Cole-Palmer) was attached to piezometer tubing and porewater slowly pumped from the ground with an Alexis V3.0 peristaltic pump (Proactive Environmental Products). Salinity, pH, and temperature were measured in a flow-through cell on a YSI sonde (600XL); during sample collection the flow-through cell was placed before the pump to reduce introduction of oxygen by pumping. Dissolved oxygen (DO) was measured with either a YSI (600XL) or a HACH (HQ40d meter with LDO101 Luminescent/Optical DO sensor). Samples for nutrient analyses were filtered with a 0.45 µm disposable groundwater filter capsule (Millipore Sigma), immediately placed on ice, transported to

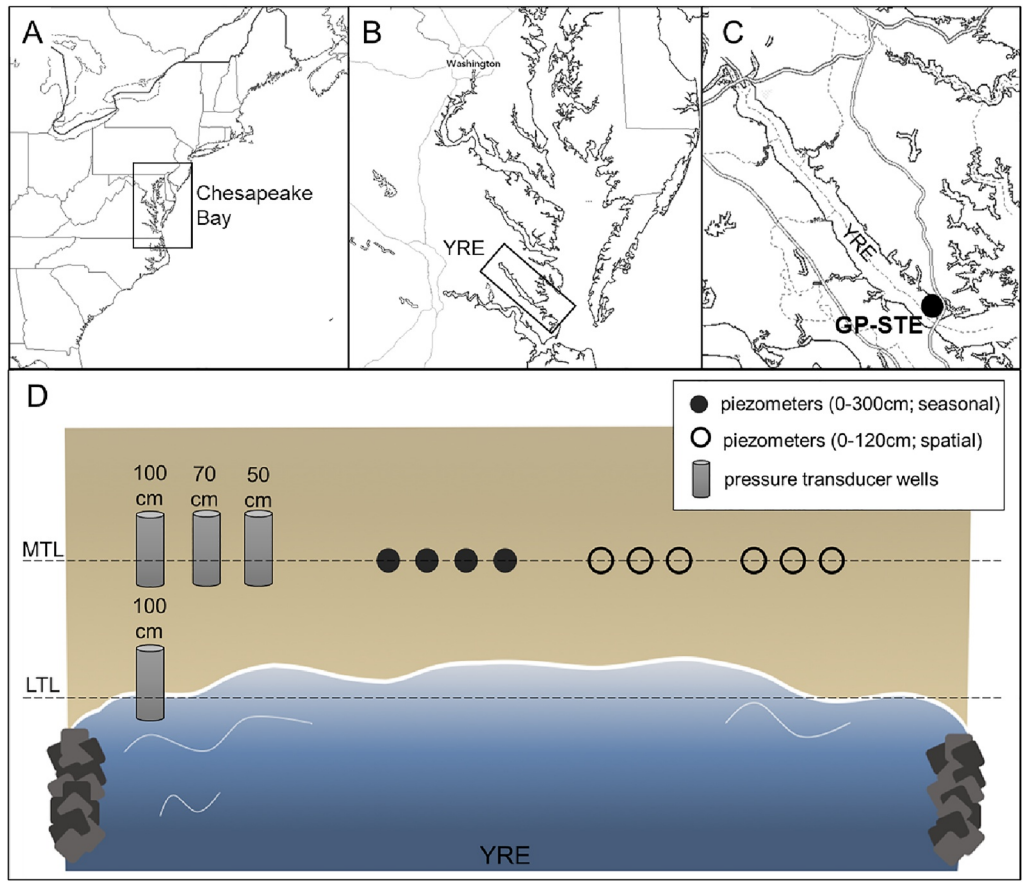

Figure 1. Site map and experimental design. (a) Map of the east coast of the USA with box denoting location of the Chesapeake Bay, (b) map of Chesapeake Bay with a box around the York River Estuary (YRE), and (c) map of YRE with study site indicated (Gloucester Point STE [GP-STE], black dot) 37.248884°N, 76.505324°W; (ArcGIS online). (d) GP-STE Sampling Scheme: Piezometers (circles) were constructed at the mid-tide line (MTL) of the Gloucester Point-Beach. All piezometers shown were sampled once at low tide to determine spatial variability (0–120 cm). Piezometers were sampled across seasons (filled circles, depths: 0–300 cm) and over two tidal cycles (filled circles, depths: 0–120 cm). Three pressure transducer wells were placed at the MTL at three depths (100, 70, and 50 cm); one well was placed at the low-tide line at 100 cm.

the lab and frozen until analysis. Porewater analyses included: DIN, DIC, phosphate (PO_4^{3-}), dissolved organic carbon (DOC), and sulfide (H_2S). DIN (NO_3^-, NO_2^-, and NH_4^+) and PO_4^{3-} concentrations were determined on a Lachat autoanalyzer (Lachat Instruments, Lachat QuikChem FIA+ 8000). DIC samples were collected unfiltered in 12 mL exetainer vials (Labco) containing 1.2 µL of saturated $HgCl_2$ solution and analyzed within 30 days of collection with an Apollo AS-C3 analyzer with a LiCor 7000 infrared CO_2 analyzer. DOC samples were filtered into pre-combusted (500°C for 5 hr) scintillation vials, stored frozen, and analyzed on a Shimadzu TOC-Vcsn analyzer. Sulfide samples were collected, filtered with 0.45 µm Puradisc membrane syringe filters (GE Healthcare Life Sciences), into 0.1 M Zinc acetate preventing exposure to air. In the lab sulfide samples were quantified spectrophotometrically (Shimadzu UV-1800) as described by Hines et al. (1989). Field instruments were calibrated the day prior to use in the field following manufacturer's instructions. All sample analyses included standard curves and check standards every 10–12 samples to assess and correct for instrument drift.

2.4. Spatial and Tidal Porewater Geochemical Monitoring

To assess spatial variability, three porewater profiles were collected from five depths (20, 50, 70, 100, and 120 cm, 15 piezometers total) and surface YRE water (0 cm) during low tide. Tidal variability samples were collected from one porewater profile (5 depths: 20, 50, 70, 100, and 120 cm) at the MTL and surface YRE water (0 cm), sampled at three tidal stages, during two tidal cycles (May and June 2020). Sample salinity, temperature, DO, NO_3^-, NO_2^-, NH_4^+, PO_4^{3-}, and DIC were collected and analyzed as previously described.

2.5. Potential N Removal Rate Incubations

A vibracore was used to collect sediment from the STE at the MTL adjacent to the dedicated piezometers. Cores were collected during seasonal sampling efforts (spring, summer, fall, winter) resulting in four cores, each 110 cm in length. Cores were sectioned at 10 cm intervals and homogenized. Approximately 1 g of the composited sediment from each 10 cm section was used in sediment slurry incubation experiments to measure denitrification and anammox rates. Samples were incubated for 6, 12, or 24 hr in sealed, helium flushed 12 mL exetainer vials (Labco) at the measured *in situ* temperature. Denitrification rate incubations were amended with 100 nmoles $^{15}NO_3^-$ (99 atm%, Cambridge Isotope Laboratories, Inc.), and $^{29,30}N_2$ products were measured using a gas bench isotope ratio mass spectrometer (IRMS, Delta V Plus, Thermo Fisher Scientific, Waltham, MA). To measure potential anammox rates, 500 nmoles of $^{15}NH_4^+$ (99 atm%, Cambridge Isotope Laboratories, Inc.) and 100 nmoles $^{14}NO_2^-$ were added to the sediment slurries; the production of $^{29}N_2$ was measured by IRMS. N_2 production rates were calculated using the methods described by Song and Tobias (2011). All incubations were conducted in duplicate.

2.6. Darcy Discharge Calculations

Three pressure transducer wells were constructed out of PVC with 10 cm of slotted PVC centered at 50, 70, and 100 cm depths along the MTL and one at 100 cm depth along the low-tide line (Figure 1d). An additional pressure transducer was installed to measure barometric pressure in a dry well above the dune line. Pressure measurements were made with a HOBO water level logger (ONSET, U20L) and recorded a measurement every 15 min; well water level was calibrated with manual measurements at logger deployment and collection. Discharge rates were calculated from head measurements made at 15-min intervals and then averaged over each month sampled. Darcy discharge was calculated using Equation 1 shown below:

$$q = -k_{h,v}\frac{dh}{dx,z} \quad (1)$$

Where q is the specific groundwater discharge (cm d^{-1}), $k_{h,v}$ is the hydraulic conductivity (horizontal, k_h, or vertical, k_v, cm/s), dh is the hydraulic head (m) determined by pressure transducer data, and (dx) is horizontal distance (m) between two wells positioned normal to the shoreline and (dz) is the vertical distance (m) between two wells at different depths at the same location. Hydraulic conductivity (k_h) of GP-STE sediment was $k_h = 0.00094$ cm/s, measured with a slug test in the 50 cm well and calculated using the Hvorslev (1951) method (Figure S2 in Supporting Information S1). This is on the same order of magnitude as the value ($k_h = 0.0001$ cm/s) reported by Reay (2009) and used by Beck et al. (2016) at this site. This measured hydraulic conductivity (k_h) also falls within the range of values reported for medium to coarse grained sand (Domenico & Schwartz, 1990). To further assess the potential variability in hydraulic conductivity at this site, the grain size of sediment samples collected at the GP-STE was measured with a laser diffraction particle size analyzer (LDPSA, model: LS 13 320, Beckman Coulter; Table S1 in Supporting Information S1). The hydraulic conductivity was calculated from grain size using the Hazen (1917) method and ranged from 0.000010 to 0.067 cm/s; the average of all grain size estimates of k_h was 0.026 ± 0.0069 cm/s (Table S2 in Supporting Information S1). Fluxes reported here are calculated with $k_h = 0.000105 \pm 0.0000026$ cm/s, which represents the first quartile of hydraulic conductivities measured at this site, and the ~28% error inferred from all estimates of k_h, which was propagated through the flux estimations. This k value represents the lower 25% of hydraulic conductivities measured which could limit flow in the STE, is on the same order of magnitude as the hydraulic conductivity measured via the slug test, and falls within the range of values measured at this site and nearby locations (Beck et al., 2016; Reay, 2009; Tobias et al., 2001). The vertical hydraulic conductivity (k_v) was assumed to be 0.1x the horizontal hydraulic conductivity (k_h) to account for sediment anisotropy, resulting in a vertical hydraulic conductivity of $k_v = 0.0000105$ cm/s (Tobias et al., 2001). To assess the effect of hydraulic conductivity on discharge estimates we conducted a sensitivity analysis and calculated horizontal groundwater discharges using the lowest k_h estimated by grain size, the k_h value estimated with the slug test in this study, the k_h value used to estimate reported fluxes, and the highest k_h value estimated by grain size (Figure S3 in Supporting Information S1).

Horizontal discharge was calculated using the hydraulic head differences between pressure transducers at 100 cm depth in the wells at the mid-tide and the low-tide lines. Vertical discharge was calculated using hydraulic head differences between 70 and 50 cm pressure transducer wells at the MTL. For each measurement within a sampled

month, the discharge in each direction was calculated (Equation 1). The total groundwater discharge was assumed to be the sum of the horizontal and vertical discharge (Tobias et al., 2001). As previously noted, discharge rates were calculated from head measurements made at 15-min intervals and were averaged for each month sampled resulting in an average total discharge for spring, summer, and fall of 2018, winter of 2019, and spring and summer of 2020. Discharge was compared to tidal height fluctuations collected by the Virginia Estuarine and Coastal Observing System (VECOS) from the GP Continuous Monitoring station (Anon, 2022).

2.7. Potential Discharge of Nutrients in SGD to the Overlying Water

Potential net fluxes of DIN ($NO_3^- + NO_2^- + NH_4^+$), and PO_4^{3-} in SGD to the overlying water were calculated using the SGD rate determined by Equation 1 and the STE endmember nutrient concentration. Calculations were performed similarly to Beck et al. (2016) but account for nutrient concentrations in the overlying water using Equation 2:

$$F = \left(C_{gw} - C_{sw}\right) * Y \tag{2}$$

where F is the net nutrient flux (mmoles m^{-2} d^{-1}) via SGD to the overlying water, C_{gw} is the shallow (50 cm) or deep (300 cm) groundwater endmember concentration (mmoles L^{-1}), C_{sw} is the surface water (0 cm) concentration (mmoles L^{-1}), and Y is the total SGD rate (L m^{-2} d^{-1}) measured in each season. Nutrient fluxes were calculated for each hydraulic gradient measurement (every 15 min) and averaged across the month sampled.

Two endmember concentrations (C_{gw}) were used to determine potential fluxes from the GP-STE including a deep, fresh groundwater endmember (300 cm) and a shallow groundwater endmember (50 cm). The deep endmember represents the DIN and PO_4^{3-} concentrations in low salinity (salinity <5) groundwater that, if transported conservatively, would be exported to the overlying York River. The shallow endmember concentration (50 cm) represents the top of the STE mixing zone, and has a similar salinity to SGD collected in seepage meters at this site by Beck et al. (2016). A study conducted by Kroeger et al. (2007), along another tributary of the Chesapeake Bay, also used nutrient concentrations at 50 cm as the SGD endmember. The shallow endmember is meant to be representative of the solutes in SGD, which have already undergone biogeochemical transformations in the STE.

To account for N removal via denitrification in the GP-STE prior to discharge, two N removal scenarios were considered. The first scenario assumes denitrification occurred only in the anoxic zone of the STE; depths where DO < 5 mg/L (Anoxic DNF). The second scenario accounts for total potential N removal throughout the STE profile; potential N removal rates observed in both the oxic and anoxic zones, to account for denitrification that may be occurring in microsites or small anoxic patches throughout the STE profile (Total DNF). To apply these scenarios, the N removal rate was accounted for in Equation 3 as:

$$F = \left(\left(C_{gw} - \left(C_{gw} * D_{dnf}\right)\right) - C_{sw}\right) * Y \tag{3}$$

Where F is the net flux after accounting for denitrification (mmoles m^{-2} d^{-1}), C_{gw} is the shallow (50 cm) groundwater endmember concentration (mmoles L^{-1}), D_{dnf} is the percent reduction by denitrification in either the anoxic portion of the STE (Anoxic DNF) or the top 1m of the STE (Total DNF), C_{sw} is the surface water (0 cm) concentration (mmoles L^{-1}), and Y is the total SGD rate (L m^{-2} d^{-1}) for the respective season. The percent reduction by denitrification is derived from the potential rate measurements in sediment slurry incubation experiments (Section 2.3) and estimated by calculating a percent of the N in the STE that could be reduced by denitrification using the measured DIN concentrations and N removal rates.

2.8. Statistical Analyses

We assessed the effect of season, tidal stage, site, and depth on porewater geochemical parameters (salinity, DO, NO_3^-, NH_4^+, DIP, and DIC concentrations) using multiple analysis of variance (ANOVA). The ANOVA included fixed effects of season (spring, summer, fall, and winter), tidal stage (low tide, mid tide, high tide), location across the beach (profile A, B, and C), and depth. A post-hoc Tukey multiple comparisons of means was used to determine how geochemical parameters varied across these scales with 95% confidence intervals. The same statistical methodology was used to assess the fixed effect of season and month on total groundwater discharge as well as the effect of season on STE sediment denitrification and anammox rates. Pearson correlation was used

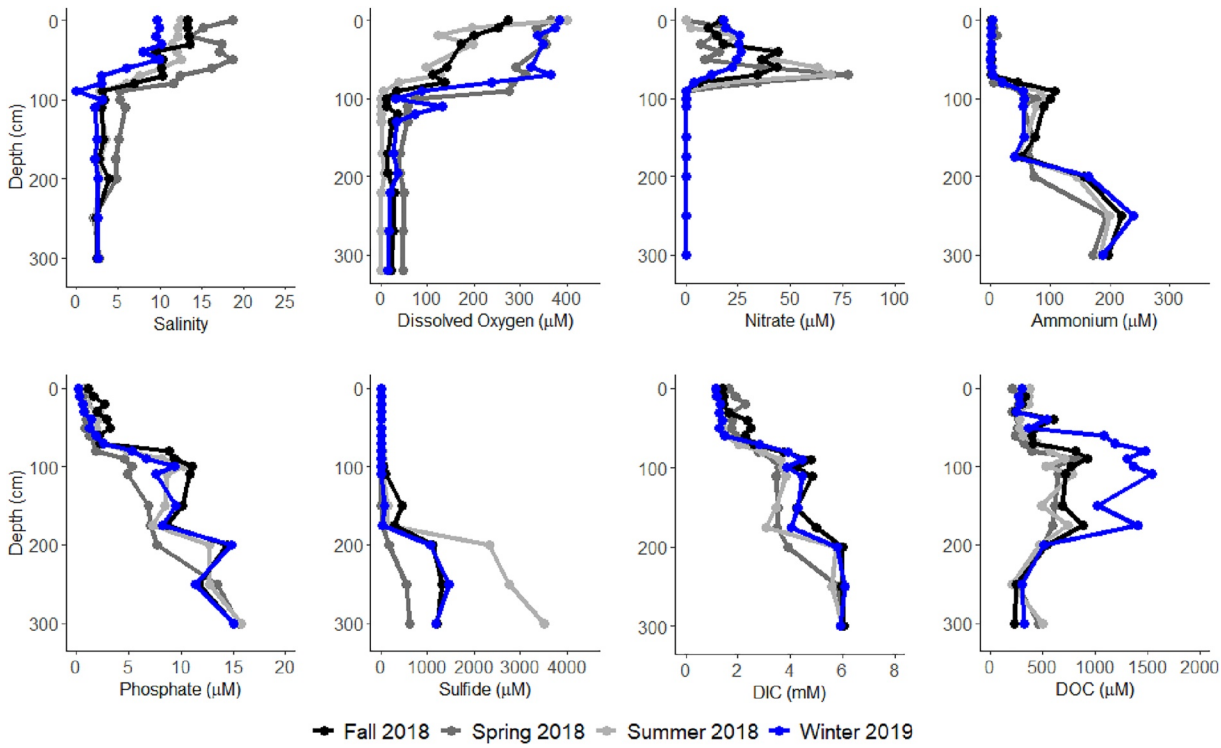

Figure 2. Gloucester Point STE porewater profiles of (a) Salinity, (b) dissolved oxygen (μM), (c) Nitrate (μM), (d) Ammonium (μM), (e) Phosphate (μM), (f) Sulfide (μM), (g) dissolved inorganic carbon (mM), and (h) dissolved organic carbon (μM) measured in fall, spring, summer, and winter (seasonal survey).

to assess relationships between geochemical analytes in the STE. All statistical analyses were conducted in R (version 3.2.2. Copyright 2015 The R Foundation for Statistical Computing) and the significance level for all statistical tests was $\alpha = 0.05$.

3. Results

3.1. Seasonal Variation in STE Porewater Geochemical Profiles

Porewater salinity decreased with depth (p-value < 0.05, Table S3 in Supporting Information S1), but gradients in the STE varied across seasons (p-value < 0.05, Figure 2a). Overlying water (0 cm, YRE water) salinity ranged from 9.7 to 19 across all seasons; the lowest salinity in overlying water coincided with the high precipitation in the area during the summer of 2018 (Figure S1 in Supporting Information S1). Increased precipitation can freshen the overlying York River water and, therefore, influence porewater salinity observed in the STE. Salinity across seasons ranged from 9.0 to 19 at 50 cm and 2.5 to 2.8 at 300 cm (deepest piezometer), suggesting that deep groundwater salinity at this site is less affected by seasonality than surficial porewaters.

Porewater DO concentrations also decreased with depth (p-value < 0.05, Table S3 in Supporting Information S1) ranging from 0.0 to 400 μM in the STE (Figure 2b). The highest DO concentrations were observed in the top 0–50 cm of the STE, followed by a decrease from 50 to 100 cm; below 100 cm porewater concentrations were consistently <160 μM (~5.0 mg L^{-1}). Lower DO concentrations were observed in summer and fall as compared to spring and winter in the top 100 cm of the STE (p-value < 0.05).

Concentrations of NH_4^+ increased with depth (p-value < 0.05) in the STE. From 0 to 100 cm, NH_4^+ concentrations were <20 μM, but increased with depth below 100 cm (Figure 2d) in all seasons. Concentrations of NO_3^- ranged from 25 to 70 μM at depths from 40 to 100 cm; whereas below 110 cm concentrations were <5.0 μM (Figure 2c). Porewater NO_3^- concentrations varied significantly with depth and season. This suggests that geochemical gradients observed and their temporal variation with depth influence NO_3^- concentrations (p-value < 0.05, Table S3 in Supporting Information S1). NO_2^- concentrations in the STE were lower than 1.7 μM in all depths and seasons (Figure S4 in Supporting Information S1).

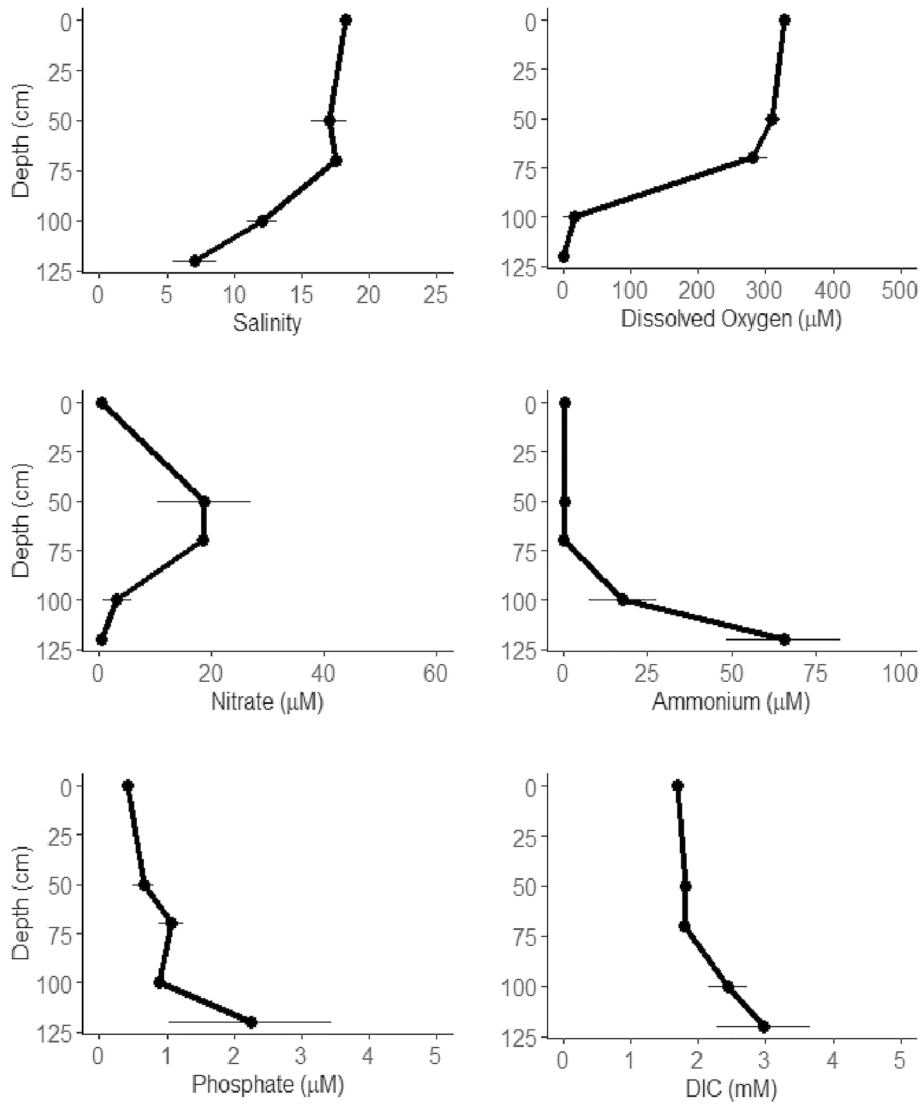

Figure 3. Mean observations of (a) Salinity, (b) dissolved oxygen (μM), (c) Nitrate (μM), (d) Ammonium (μM), (e) Phosphorus (μM), and (f) dissolved inorganic carbon (mM) collected at the mid-tide line across the beach face to assess spatial variability. Points represent the mean of three measurements at the specified depth across the beach and error bars represent one standard error in each direction.

Porewater PO_4^{3-} and DIC concentrations increased with depth in all seasons (p-value < 0.05, Figures 2e and 2g). PO_4^{3-} concentrations ranged from 0.16 to 16 μM and DIC concentrations ranged from 2.0 to 6.0 mM. Porewater PO_4^{3-} and DIC concentrations were higher in fall and winter than spring and summer (p-value < 0.05). H_2S concentrations increased with depth in every season (Figure 2f), varying from 0 to 3,500 μM. DOC concentrations in STE porewater ranged from 250 to 1,500 μM (Figure 2h). There was a consistent pattern observed in each season sampled; elevated DOC concentrations (>400 μM) were observed from roughly 80–250 cm.

3.2. Spatial and Tidal Variation in STE Porewater Geochemical Profiles

Spatial variability of porewater geochemical characteristics was evaluated by sampling three replicate profiles along the MTL of the beach (Figure 3, Figures S6 and S7 in Supporting Information S1). Profiles of salinity, DO, DIN, PO_4^{3-}, and DIC showed similar trends to those observed during seasonal sampling and variations observed with site across the beach face were not statistically different (p-value > 0.05, Table S3 in Supporting Information S1). Porewater geochemical variation was also examined throughout two tidal cycles for salinity, DO, DIN,

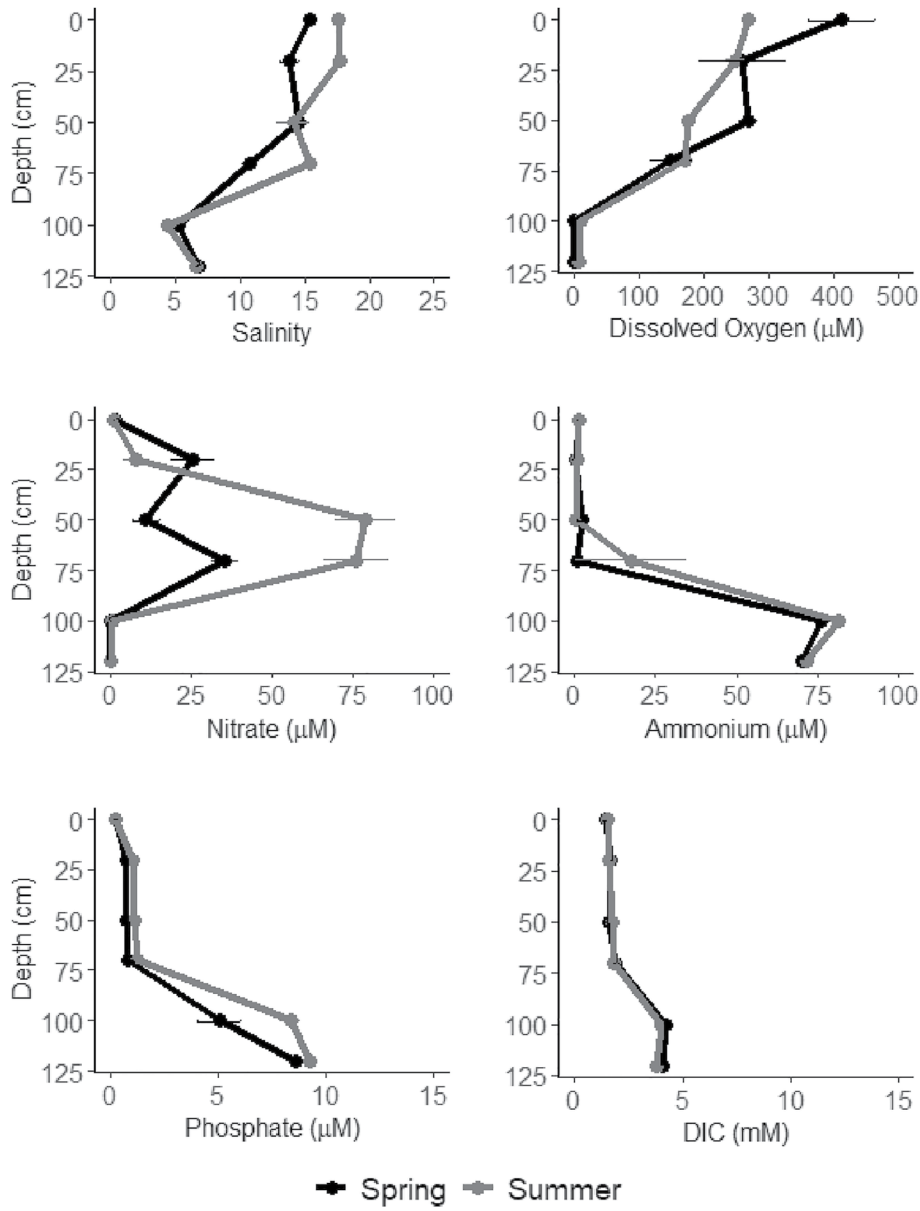

Figure 4. Mean observations of (a) Salinity, (b) dissolved oxygen (μM), (c) Nitrate (μM), (d) Ammonium (μM), (e) Phosphorus (μM), and (f) dissolved inorganic carbon (mM) collected at the mid-tide line three times throughout a tidal cycle (spring tide; sampled at high, mid, and low tide) in the spring (black) and summer (gray) of 2020 to assess tidal variability within Subterranean estuarie profiles. Points represent the mean of three measurements throughout the tidal cycle and error bars represent one standard error in each direction.

DIP, and DIC; profiles exhibited similar patterns as those observed during seasonal and spatial surveys (Figure 4, Figure S5 in Supporting Information S1). All analytes had similar concentrations and patterns with depth across tidal stages (p-value > 0.05, Table S3 in Supporting Information S1).

All porewater samples (seasonal, spatial, and tidal) were combined to assess correlations between geochemical analytes (Figure S8 and Table S4 in Supporting Information S1). There was a negative correlation between porewater salinity and NH_4^+ (p-value < 0.05) and a positive correlation between salinity and NO_3^- (p-value < 0.05). NH_4^+ and NO_3^- concentrations exhibited a negative correlation (p-value < 0.05). Porewater salinity had a positive correlation with DO; correlation coefficient = 0.78 (p-value < 0.05), but was negatively correlated with PO_4^{3-} and DIC; (p-value < 0.05). Porewater DIC and DIP had a strong positive correlation (Pearson coefficient = 0.93, p-value < 0.05). DIC also had a positive correlation with porewater NH_4^+ concentrations (p-value < 0.05).

Table 1
Potential Denitrification Rates Measured Seasonally in Sediment Slurries Using the IPT Method (Song & Tobias, 2011) in mmol N m^{-2} d^{-1} and the Associated Standard Deviation

	Spring 2018		Summer 2018		Fall 2018		Winter 2019	
Depth (cm)	Rate	Standard deviation	Rate	Standard deviation	Rate	Standard deviation	Rate	Standard deviation
0–10	0.0075	0.0090	3.6	0.49	7.9	0.57	1.8	0.11
10–20	0.022	0.025	4.3×10^{-5}	1.1	7.6	0.55	1.1	0.093
20–30	2.6×10^{-5}	5.2×10^{-5}	0.41	0.025	2.3	0.45	1.3	0.14
30–40	0.0028	0.0032	0.091	0.0082	2.7	0.49	0.88	0.030
40–50	0.0042	0.0053	0.053	0.0040	7.5	0.76	0.83	0.085
50–60	2.4×10^{-5}	2.8×10^{-5}	0.14	0.096	2.4	0.71	0.49	0.052
60–70	0.22	0.0068	0.078	0.021	1.5	0.51	0.10	0.44
70–80	6.0×10^{-6}	1.2×10^{-5}	0.55	0.18	0.64	0.20	0.45	0.11
80–90	0.0053	0.0062	0.11	0.044	0.34	0.040	0.11	0.068
90–100	0.018	0.021	0.017	0.020	3.6	0.35	0.0017	0.0095
100–110	2.4×10^{-5}	3.9×10^{-5}	0.042	0.029	0.65	0.16	0.0	0.0

3.3. Seasonal Potential N Removal Rates

In all seasons and depths, potential anammox rates were <0.064 mmol N m^{-2} d^{-1} and denitrification rates ranged from 0.0 to 7.9 mmol N m^{-2} d^{-1} (Table 1 and Table S5 in Supporting Information S1). The highest rates of denitrification were observed in the fall of 2018; lowest rates were observed in the spring of 2018 (Table S3 in Supporting Information S1, p-value > 0.05). In all seasons the highest rates of denitrification were observed in surficial sediment (0–50 cm).

3.4. Darcy Discharge Calculations

Horizontal discharge averaged for each of the sampled months ranged from 15 to 24 L m^{-2} d^{-1} and the average vertical discharge ranged from −3.4 to 67 L m^{-2} d^{-1} (Table 2). Negative vertical discharge rates were observed periodically in winter 2019 and spring 2020, this is consistent with a change in the direction of the vertical hydraulic gradient, indicative of recharge. The average total groundwater discharge ranged from 20 to 87 L m^{-2} d^{-1}; highest discharge rates were observed during summer and the lowest in winter (p-value < 0.05). The magnitude of the vertical and horizontal gradients and, therefore, total groundwater discharge fluctuated with season and tide; lower discharge rates were observed at high tide and the highest discharge was observed in summer (Figures S9 and S10 in Supporting Information S1).

3.5. SGD Nutrient Flux Calculations

Calculated fluxes of DIN and PO_4^{3-} from the GP-STE to overlying water are shown in Table 3. The SGD DIN fluxes calculated using the deep, groundwater endmember ranged from 3.3 ± 0.92 to 17 ± 4.7 mmol m^{-2} d^{-1}.

Table 2
Average Horizontal, Vertical, and Total Groundwater Discharge ± Standard Error in L m^{-2} d^{-1} for Each Season Sampled

	Spring		Summer		Fall	Winter
	2018	2020	2018	2020	2018	2019
Horizontal discharge	24 ± 6.6	22 ± 6.0	20 ± 5.5	22 ± 6.3	15 ± 4.1	23 ± 6.5
Vertical discharge	14 ± 3.9	−1.5 ± 0.42	67 ± 18	0.85 ± 0.24	27 ± 7.4	−3.4 ± 0.96
Total discharge	38 ± 11	20 ± 5.6	87 ± 24	23 ± 6.5	41 ± 12	20 ± 5.5

Note. Average of all observations of total discharge = 38 ± 11 L m^{-2} d^{-1}.

Table 3
Net Nutrient Fluxes via Submarine Groundwater Discharge for Each Season Reported in mmol m^{-2} d^{-1} ± Standard Error

Flux	Endmember scenario	Spring	Summer	Fall	Winter
DIN	Deep	7.0 ± 2.0	17 ± 4.7	5.9 ± 1.7	3.3 ± 0.92
	Shallow	0.31 ± 0.088	3.6 ± 0.97	0.35 ± 0.098	0.065 ± 0.018
	Anoxic DNF	0.31 ± 0.088	3.5 ± 0.96	0.19 ± 0.052	0.013 ± 0.0037
	Total DNF	0.31 ± 0.087	3.3 ± 0.89	−0.54 ± 0.15	−0.22 ± 0.062
PO_4^{3-}	Deep	0.58 ± 0.16	1.3 ± 0.36	0.58 ± 0.16	0.29 ± 0.082
	Shallow	0.026 ± 0.0072	0.093 ± 0.025	0.089 ± 0.025	0.019 ± 0.0052

Note. Deep endmember represents the flux estimated using DIN and PO_4^{3-} concentrations at the 300 cm depth in the STE. The shallow endmember fluxes represent those estimated using concentrations at the 50 cm depth. The anoxic zone and total DNF fluxes were calculated using the N removal scenarios described in Section 2.3.

PO_4^{3-} fluxes estimated with the deep endmember ranged from 0.29 ± 0.082 and 1.3 ± 0.36 mmol m^{-2} d^{-1}. The shallow endmember (50 cm) fluxes of DIN ranged from 0.065 ± 0.018 to 3.6 ± 0.97 mmol m^{-2} d^{-1}. The lowest and highest DIN fluxes were observed in winter and summer respectively (Table S7 in Supporting Information S1, p-value < 0.05). The groundwater PO_4^{3-} flux calculated with the shallow endmember (50 cm) ranged from 0.019 ± 0.0052 (winter) to 0.093 ± 0.025 (summer) mmol m^{-2} d^{-1} (Figure S13 in Supporting Information S1).

To account for potential N removal, the reduction of DIN by denitrification, as measured in sediment slurry incubations, was incorporated into flux estimations. Accounting for the N removal in the anoxic zone of the STE (Anoxic DNF), shallow endmember DIN fluxes are reduced 0.58%–~80% depending on the season (Table 3). Using the total N removal observed in both oxic and anoxic zones of the STE (Total DNF) shallow endmember DIN fluxes are reduced 0.67% to >100%. Denitrification exceeded the SGD N flux in fall and winter, suggesting that the STE acts as a sink for DIN during these seasons.

4. Discussion

4.1. Spatial and Temporal Variability in STE Geochemical Profiles

Variations in STE porewater profiles may be driven by location, sampling depth, season, and tidal stage. This variation determines which C and N cycling processes will occur in STEs and at what rates. In the GP-STE, although season and depth had significant effects on porewater salinity, DO, DIN, PO_4^{3-}, and DIC, location and tidal stage did not (Table S3 in Supporting Information S1). Steep geochemical gradients are common in STEs; thus, we expected to observe variation with depth. Tidal pumping has been reported as a major driver of variability in other STEs (Robinson et al., 2018); however, this does not seem to be the case in the GP-STE. Stability in geochemical profiles was observed across varying stages of tidal amplitude in this study and previous work (Beck et al., 2016). The lack of tidal variation may be the result of low groundwater flow velocity, limited wave action, and the small tidal height at this site.

Porewater salinity and DO profiles observed in the STE were as expected when oxic seawater mixes with advected anoxic groundwater. Our observations align with previous measurements of salinity, DO, and nutrient profiles at this site (Beck et al., 2016; O'Connor et al., 2015), but porewater DO penetrated deeper than has been observed in other coastal sediments which are typically anoxic within millimeters to centimeters below the sediment-water interface (Cai & Sayles, 1996). The observed DO profile could result from the high permeability of the sandy sediment in the lower YRE and periodic, high wave action from passing ships in the nearby channel (Bilkovic et al., 2019).

Groundwater supplies high concentrations of NH_4^+ (~200 μM) to the GP-STE, likely due to remineralization of organic matter during transport to the coast or contamination resulting from septic leakage (Mitchell et al., 2021). Schutte et al. (2017) reported similar NH_4^+ concentrations with depth on Sapelo Island, GA, USA, but other east coast sites such as Waquoit Bay, MA, USA observe NO_3^- rich groundwater (Spiteri, Slomp, Charette et al., 2008; Talbot et al., 2003). The lack of NO_3^- below 100 cm in the STE could be the result of low NO_3^- in the source groundwater. In addition, any NO_2^- or NO_3^- produced by anaerobic ammonium oxidation in the anoxic zone of

the STE may be consumed by nitrate reduction via denitrification or DNRA. However, as groundwater moves along its flow path and reaches the STE mixing zone, NH_4^+ concentrations decrease, coinciding with increasing NO_3^- and DO concentrations. The STE profiles and the negative correlation observed between NH_4^+ and NO_3^- concentrations suggest that the loss of NH_4^+ and production of NO_3^- is the result of nitrification. Oxidation of NH_4^+ by nitrification is typical in sandy STEs (Santos et al., 2021) and deep oxygen penetration has been proposed as a driver of nitrification of groundwater-borne NH_4^+ in sandy systems (Schutte et al., 2017); our data suggest a similar dynamic.

The profiles of PO_4^{3-}, DIC, NH_4^+, and H_2S concentrations increased with depth, which aligned with previous observations (O'Connor et al., 2018; Wu et al., 2021). The deepest groundwater samples were enriched with PO_4^{3-}, DIC, and NH_4^+. Porewater PO_4^{3-}, DIC, and NH_4^+ were negatively correlated with salinity and DIC was positively correlated with PO_4^{3-}, and NH_4^+ (Figure S8 in Supporting Information S1), suggesting these analytes are products of remineralization. H_2S also increased with depth; deep oxygen penetration in the STE likely drives less energetically favorable redox reactions, such as sulfate reduction, deeper into the sediments.

4.2. Potential N Removal Rates

Denitrification was the dominant microbial N removal pathway in the GP-STE; anammox rates were ubiquitously low. The observed denitrification rates were similar to those observed by Jiao et al. (2018) in a sandy STE in Daya Bay, China using a similar slurry incubation method, but were lower than N removal rates in some other coastal sediments (Cornwell et al., 1999; Hall et al., 2005). Denitrification has also been measured in STEs using *in situ* tracer (Addy et al., 2002; Tobias et al., 2001) and flow-through experiments (Wong et al., 2020), which resulted in higher rates than those observed in this study. Incubations were conducted at *in situ* STE temperature and the highest denitrification rates were observed in fall despite the highest temperatures being observed in summer. This does not align with a positive temperature effect on denitrification and suggests that another factor limits rates such as labile organic matter or substrate availability. GP-STE sediments have only ~0.26% organic content (determined by combustion of dried sediment, unpublished data), so that the availability of organic matter may be a limiting factor. The organic matter that is available may also be recalcitrant; O'Connor et al. (2015) observed that 43% ± 18% of the total GP-STE DOC pool was comprised of humic material, indicative of low lability. Low concentrations of oxidized DIN, which is required for anammox and denitrification, in the anoxic zone of the GP-STE would also limit N removal *in situ*. The NO_3^- profile (Figure 2c) showed no NO_3^- below 100 cm where the anoxic zone begins and NH_4^+ concentrations begin to increase, which could be the result of denitrification of any available NO_3^-, but the observed low potential rates suggest minimal N removal occurring deep in the STE.

Most calculations of SGD nutrient fluxes do not account for transformations or removal along the groundwater flow path (Beck et al., 2016; Charette & Buesseler, 2004; Correa et al., 2020). Despite the difficulty of accurately estimating STE transformations, unaccounting for these processes can lead to overestimations or underestimations of nutrient fluxes via SGD as these transformations may remove (i.e., denitrification or sorption) or produce (i.e., remineralization) inorganic nutrients. Our slurry incubations were performed under anoxic conditions with excess NO_3^- and, therefore, do not account for *in situ* oxygen and substrate concentrations. However, these observations do provide potential rates under optimal conditions for these processes. Potential rates are typically considered over-estimations, but can be useful to calculate a potential "maximum" N that could be removed in the STE. Since denitrification is an anoxic process and increased oxygen availability decreases denitrification rates (Bonin & Raymond, 1990; Seitzinger et al., 2006), it is likely that STE N removal would occur mainly at depths that exhibit low oxygen or anoxic conditions. If we assume that denitrification would not occur above 60 cm, where >5 mg/L DO is observed (Oh & Silverstein, 1999), the maximum N removal in the top 1 m^3 would be ~1,500 μmol N m^2 d^{-1}. This is approximately 20% of the available NO_3^- pool in the top 1 m^3 of the STE (~7,400 μmol N). Much of the N pool, therefore, would be available for discharge to the overlying water. However, the highest potential rates of denitrification and anammox at this site were observed in surficial sediments. The surficial STE sediments are oxic, which may inhibit denitrification, but the oxic region is closer to labile organic matter provided by overlying water and it is possible that N removal is occurring in anoxic microsites or patches (Arango et al., 2007). Despite the low observed rates, the maximum N removal in both oxic and anoxic zones of the sediment profile, would attenuate the entirety of the STE DIN pool in fall and winter and result in a ~80% DIN pool reduction in summer and spring. The true rate of N removal in the STE is likely somewhere between this 20% and 100% removal; a ^{15}N labeled *in situ* tracer experiment conducted at the GP-STE

indicated denitrification in surficial sediments (50 cm) of less than 0.075 mmoles N m^{-2} d^{-1} suggesting that denitrification in the oxic zone is not a major contribution *in situ* (Wilson, 2022). Considering that high rates of attenuation by denitrification would require anoxic conditions and that NO_3^- is observed in surficial porewaters, our data suggest that at least some NO_3^- is released to the overlying water. However, N removal rates observed at our site have the potential to partially or fully attenuate DIN prior to discharge and this reduction should be considered in flux calculations so as to not overestimate DIN export via SGD.

4.3. Groundwater Discharge

Hydraulic gradients in the GP-STE indicated groundwater discharge to the YRE. Variation following the tidal cycle observed in hydraulic gradients at the GP-STE was in contrast with our tidal survey of geochemical profiles, which suggested minimal effect of tidal cycles (Figures S9, S10, and Table S3 in Supporting Information S1). STEs are dynamic systems that, in addition to tidal and seasonal impacts, may also be influenced by landward and seaward forces (Slomp & Cappellen, 2004). Factors such as rainfall and wave action are likely to affect groundwater flow in the GP-STE. The flow of groundwater will, in turn, impact STE geochemistry and nutrient cycling rates, and thus STE variability. As previously noted, discharge calculations can be highly sensitive to hydraulic conductivity (k) as shown by the sensitivity analysis (Figure S3 in Supporting Information S1), which highlights that discharge estimates are directly related to the magnitude of k. Spatial variation in hydraulic conductivity throughout the lower YRE would also influence groundwater discharge rates (Taniguchi et al., 2003).

We observed groundwater discharge to the overlying York River in all seasons. The calculated discharge rates are of the same order of magnitude as those previously estimated for the GP-STE by Beck et al. (2016; 3.9–6.2 cm d^{-1}; i.e., 39–62 L m^{-2} d^{-1}). Horizontal hydraulic gradients were observed consistently in the STE, indicating that water was moving outward from land, but vertical hydraulic gradients varied with season. Negative vertical gradients, indicating recharge or movement of the seepage face, were observed periodically in winter 2019 and spring 2020. These negative vertical gradients could result from lower rainfall during the winter months leading to lower groundwater flow. Higher tidal heights observed in winter may also increase the pressure from the overlying water, decreasing groundwater flow; the reversal of hydraulic gradients in the subsurface contributes to typically high variability in STE profiles (Moore, 1999). Changes in the direction of the hydraulic gradient may also indicate a shift in the location of the discharge zone along the beach face. The period of highest groundwater discharge, summer 2018, was also a period of high rainfall in the area suggesting that the magnitude of discharge may be dominantly controlled by seasonal watershed hydrology rather than shorter-term tidal drivers.

4.4. Potential Nutrient Fluxes

Nutrient fluxes via groundwater were calculated in several ways including the use of a deep endmember, assuming conservative transport of nutrients, and a shallow endmember (50 cm), to represent STE mixing zone concentrations, and two scenarios that account for potential microbial N removal prior to discharge (Table 3). The deep endmember DIN and PO_4^{3-} fluxes were the largest as the deep groundwater is enriched with inorganic nutrients. Using a groundwater endmember and assuming conservative transport has traditionally been the approach for groundwater flux studies; however, this may overestimate nutrient fluxes. This approach does not account for microbial processing, removal, or sorption in the STE where nutrients are often transformed, produced, or consumed. The shallow endmember (50 cm) represents the nutrient concentrations at the top of the STE mixing zone, likely these concentrations represent nutrient concentrations post-processing and may be a better estimate of SGD export, but there is still potential for N removal during discharge. In our analysis, accounting for potential denitrification in the STE significantly reduced DIN fluxes, underscoring the importance of N removal along the groundwater flow path.

Our estimated SGD nutrient fluxes for the GP-STE site fall within the range of those previously reported other coastal systems (Table S6 in Supporting Information S1). DIN and PO_4^{3-} fluxes (Shallow Endmember) were of the same order of magnitude as those previously calculated for the GP-STE and the Elizabeth River, another tributary of the Chesapeake Bay (Beck et al., 2016; Charette & Buesseler, 2004). Reay et al. (1992) reported higher DIN discharge from groundwater to the Chesapeake Bay (~260 mmoles DIN m shoreline^{-1} d^{-1}, assuming a shoreline of 1.86 × 107 m); however, they used seepage meters to determine groundwater discharge, which can induce flow under certain conditions (Rosenberry et al., 2008). Nutrient fluxes at the GP-STE were of

similar magnitude to those observed at Point Judith Rhode Island, USA (Scott & Moran, 2001), Bangenden Beach, Indonesia (Adyasari et al., 2019), and Sydney Harbor, Australia (Correa et al., 2020) all of which are urban coastal areas as well as to estuaries including the North Inlet South Carolina, USA (Krest et al., 2000) and Tauranga Harbor in New Zealand (Stewart et al., 2018). However, the SGD-derived N and P fluxes observed in this study were lower than those observed in Sanggou and Sansha Bays in China (G. Wang et al., 2018; X. Wang et al., 2014), Gamak Bay in Korea (Hwang et al., 2010), and Nauset March Estuary, MA, USA. SGD (Portnoy et al., 1998). SGD derived nutrients are relevant in many regions across global coastlines (Cho et al., 2018; Santos et al., 2021) and, despite many local efforts to measure nutrient fluxes, they often remain overlooked in assessments of coastal biogeochemistry and nutrient budgets (Gruber & Galloway, 2008; Lake & Brush, 2015).

SGD commonly has higher N:P ratios than Redfield (Santos et al., 2021). In some cases the N:P ratio of SGD is >50, which far exceeds the stoichiometry found in the two tributaries draining into the YRE; the Pamunkey (average DIN:DIP ratio = 13 ± 1.6) and the Mattaponi (average DIN:DIP ratio = 16 ± 1.6) (CBNERR-VA VIMS, Virginia Estuarine and Coastal Observing System (VECOS), 2021). It has been hypothesized that the high N:P ratios found in SGD may cause systems to become P rather than N-limited (Santos et al., 2021; Slomp & Cappellen, 2004). The average inorganic DIN:DIP ratio of the YRE itself is 40 ± 12 and fluctuates seasonally; exhibiting N limitation in the summer and fall and P limitation in winter (Killberg-Thoreson et al., 2013; Sin et al., 1999; Stanley, 2021). Our data suggest that the DIN:DIP ratio of groundwater, calculated using the shallow endmember, varies with season. The summer and winter SGD exhibited DIN:DIP ratios exceeding the Redfield ratio, whereas in spring 2018 and fall 2019 SGD N:P ratios were closer to Redfield. Despite reported N limitation in the summer, the lower YRE exhibits annual algal blooms. High SGD rates coupled with the high porewater DIN concentrations observed in summer, result in higher fluxes of DIN via SGD, coincident with annual summer HAB events (Reay, 2009). It is important to account for SGD as a source of high DIN:DIP water that differs from other nutrient sources, as this will influence biogeochemistry and may stimulate primary production in the overlying water.

Along with SGD, estuaries receive N and P from their tributaries, watershed runoff, and diffusive benthic fluxes that release nutrients to the water column. To compare sources within the YRE, fluvial and benthic fluxes of DIN and DIP from previous work (Lake & Brush, 2015; Woods, 2021) were extrapolated to the area of the lower York River for comparison to SGD. The fluvial DIN and DIP fluxes, which represent nutrient loading flowing downstream, were outputs of a water quality model developed and described by Lake and Brush (2015) for the YRE (reported 5.4% error between modeled and measured chlorophyll-a concentrations). The model separates the YRE into several boxes and the fluvial flux used here represents the nutrients flowing in YRE surface water from Box 7 to Box 8 (Lake & Brush, 2015), this flux was extrapolated to the entire area of the lower YRE (Box 8, 47.88 km^2, Figure S11 in Supporting Information S1). The diffusive benthic fluxes of DIN and DIP were determined experimentally with whole core incubations conducted seasonally in 2019 and 2020 (Woods, 2021). The diffusive benthic fluxes measured in the lower portion of the YRE, were extrapolated to the same area. The SGD fluxes determined in this study were extrapolated to a seepage zone defined as 40 m on either side of the river. This was based on seepage meter measurements by Beck et al. (2016) and includes discharge rates exponentially decreasing with distance from the shoreline. The width of the seepage zone was determined as the boundary of Box 8 from Lake and Brush (2015) with a 40 m buffer split into three zones 0–10, 10–20, and 20–40 m (Figure S12 in Supporting Information S1) and calculated in ArcGIS. SGD DIN and PO_4^{3-} discharge rates were extrapolated to the area of the seepage zone, accounting for exponential decline in SGD moving outward from shore, for comparison to the diffusive benthic and fluvial sources (Figures 5 and 6, Table S6 in Supporting Information S1).

The fluvial fluxes were the largest source of inorganic nutrients to the lower YRE in all seasons, this flux was an order of magnitude higher than both benthic and SGD fluxes (Figures 5 and 6). Our data, therefore, suggest that riverine transport downstream in the lower YRE is the dominant source of inorganic nutrients to this system. It is possible that a portion of these nutrients transported in YRE surface water may be the result of SGD upstream, as groundwater discharge has been observed along the length of the river (Luek & Beck, 2014). The highest estimate of potential SGD fluxes, calculated using the deep endmember approach, was roughly 4%–11% and 1%–4% of the fluvial DIN and PO_4^{3-} fluxes, respectively. Diffusive benthic fluxes represented net uptake of N in spring, fall, and winter in the YRE, which may be the result of benthic microalgae. This may also attenuate SGD derived nutrients as SGD flows through surficial sediments and, when combined with microbial N removal in the STE, SGD derived nutrients may be completely attenuated prior to discharge in spring, fall, and winter. In the summertime, DIN was released from the benthos and SGD derived DIN was not completely attenuated by

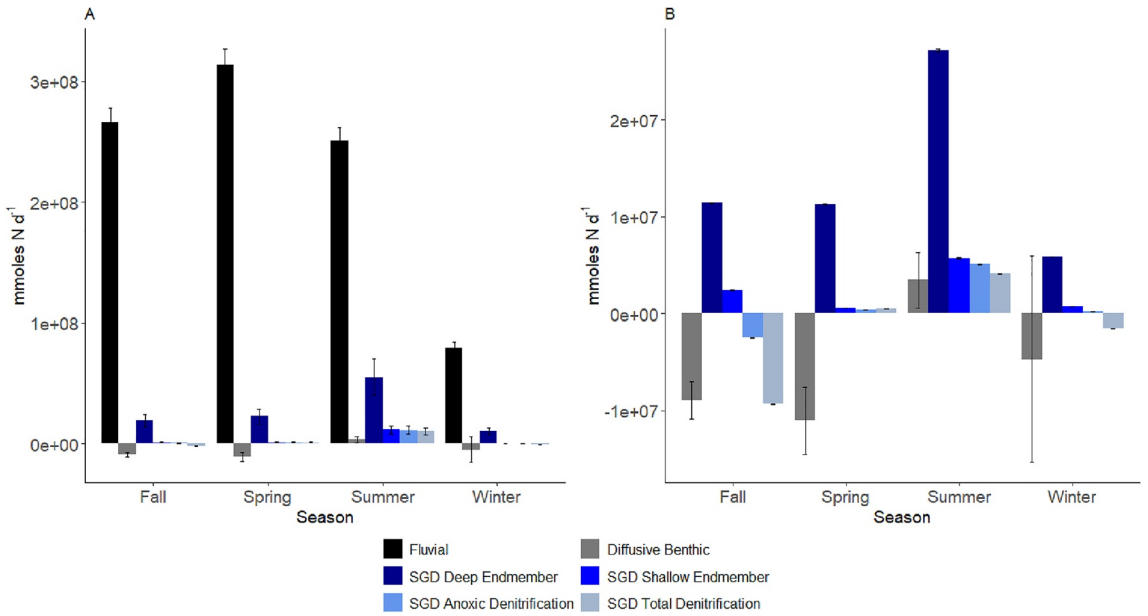

Figure 5. Comparison of fluvial (black), diffusive benthic flux (gray), submarine groundwater discharge (SGD) deep endmember flux (dark blue), and SGD shallow endmember flux (blue), SGD anoxic denitrification scenario flux (light blue), and SGD total denitrification scenario flux (periwinkle) of dissolved inorganic nitrogen in the lower York River Estuary. (a) shows all calculated fluxes and panel (b) shows all fluxes except the advective flux. Error bars represent one standard error in each direction.

STE N removal, so SGD serves as additional source of DIN during the summer months. DIP diffusive benthic fluxes were negligible with no discernible uptake or release of P suggesting little or no uptake of SGD derived PO_4^{3-} by the benthos. This extrapolation exemplifies the magnitude of SGD fluxes in this location but applies widely to other coastal systems (Table S8 in Supporting Information S1), where SGD may also be a source of inorganic nutrients. There is likely temporal and spatial variability in the rate of groundwater discharge along the

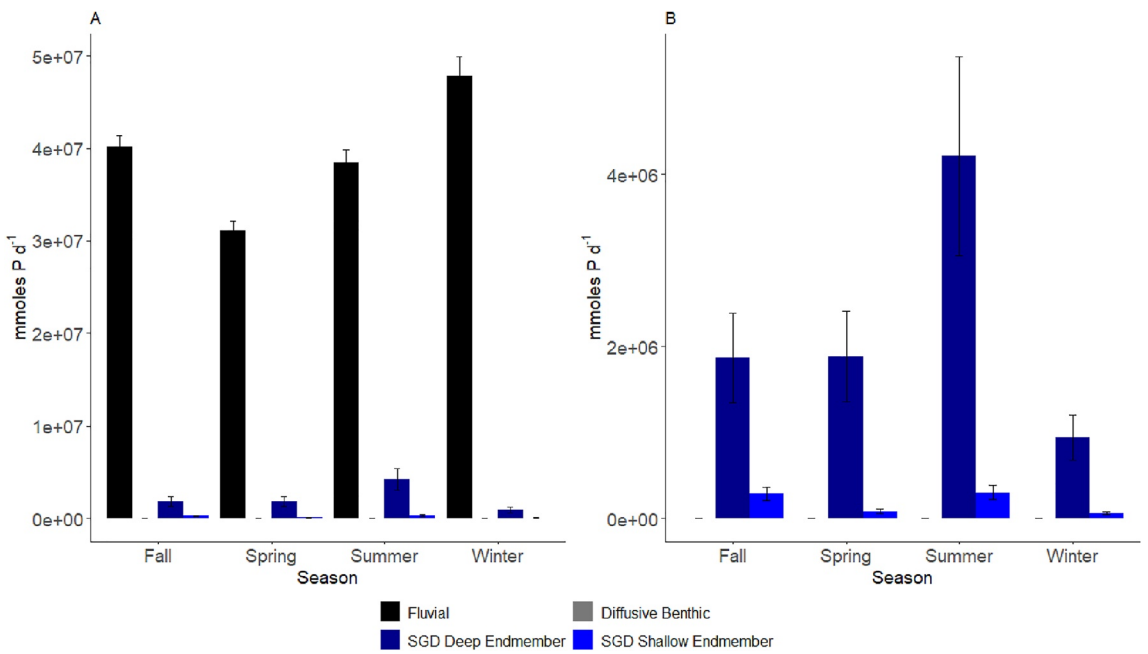

Figure 6. Comparison of advective (black), benthic flux (gray), submarine groundwater discharge (SGD) deep endmember flux (dark blue), and SGD shallow endmember flux (blue) of PO_4^{3-} in the lower York River Estuary. (a) Shows all calculated fluxes and panel (b) shows all fluxes except the advective flux. Error bars represent one standard error in each direction.

entire YRE, but our observations indicate that the GP-STE is a net source of nutrients to the overlying water in summer despite N removal and uptake.

STEs act as biogeochemical reactors for groundwater and surface water and are important transition zones along the land-ocean continuum. Our data reveal how biogeochemical cycling in STEs can significantly influence SGD nutrient loading. At this site, groundwater delivers high concentrations of dissolved inorganic nutrients to the STE where they may be transformed or attenuated, by both biotic and abiotic processes such as nitrification, denitrification, and sorption to sediments, prior to discharge to the overlying water. In the lower portion of the YRE, during the fall, and winter, nitrification and subsequent denitrification in the STE may protect the YRE from high nutrient groundwater discharge. Despite the maximum potential N removal by denitrification in the STE, SGD was a source of nutrients to the YRE in spring and summer. SGD has been reported as an appreciable source of nutrients to some estuaries and coasts, which may cause eutrophication and formation of HABs (Santos et al., 2021). In the lower YRE, SGD appears to be a small source as compared to riverine transport especially after accounting for N removal in the STE. As groundwater nutrient fluxes are further constrained, reactions in STEs altering SGD export should be considered to better estimate groundwater nutrient loading. This will determine whether groundwater should be included in future water quality models and when investigating drivers of coastal zone primary production and biogeochemistry.

Conflict of Interest

The authors declare no conflicts of interest relevant to this study.

Data Availability Statement

Data referred to in this manuscript have been made publicly available via the BCO DMO data repository site. Any other materials can be made available by the corresponding author. Data from this manuscript can be found at the BCO DMO project site (https://www.bco-dmo.org/project/805722) and includes seasonal, spatial, and tidal geochemical profile data (https://www.bco-dmo.org/dataset/807664/data, https://doi.org/10.26008/1912/bco-dmo.807664.2), sediment incubation data (https://www.bco-dmo.org/dataset/886227/data, https://doi.org/10.26008/1912/bco-dmo.886227.1), water level data from pressure transducer wells monitoring groundwater levels (https://www.bco-dmo.org/dataset/886319/data, https://doi.org/10.26008/1912/bco-dmo.886319.1), slug test water level data from pressure transducer well (https://www.bco-dmo.org/dataset/894312, https://doi.org/10.26008/1912/bco-dmo.894312.1), and sediment grain size data (https://www.bco-dmo.org/dataset/894323, https://doi.org/10.26008/1912/bco-dmo.894323.1).

Acknowledgments
This study was funded by the National Science Foundation (1658135 and 1737258) and the Virginia Institute of Marine Science. We thank Hunter Walker and Michele Cochran at the Virginia Institute of Marine Science (VIMS) for their assistance with field work, nutrient analyses, and IRMS maintenance. We also thank Dr. Chris Hein and Jennifer Connel (VIMS) for aid in sediment vibracore collection and grain size analysis.

References

Addy, K., Kellogg, D. Q., Gold, A. J., Groffman, P. M., Ferendo, G., & Sawyer, C. (2002). In situ push–pull method to determine ground water denitrification in riparian zones. *Journal of Environmental Quality*, *31*(3), 1017–1024. https://doi.org/10.2134/jeq2002.1017

Adyasari, D., Oehler, T., Afiati, N., & Moosdorf, N. (2019). Environmental impact of nutrient fluxes associated with submarine groundwater discharge at an urbanized tropical coast. *Estuarine, Coastal and Shelf Science*, *221*, 30–38. https://doi.org/10.1016/j.ecss.2019.03.009

Anderson, D. M., Glibert, P. M., & Burkholder, J. M. (2002). Harmful algal blooms and eutrophication: Nutrient sources, composition, and consequences. *Estuaries*, *25*(4), 704–726. https://doi.org/10.1007/BF02804901

Andrisoa, A., Stieglitz, T. C., Rodellas, V., & Raimbault, P. (2019). Primary production in coastal lagoons supported by groundwater discharge and porewater fluxes inferred from nitrogen and carbon isotope signatures. *Marine Chemistry*, *210*, 48–60. https://doi.org/10.1016/j.marchem.2019.03.003

Anon. (2022). *NOAA national estuarine Research Reserve system (NERRS). System-wide monitoring Program*. Data accessed from the NOAA NERRS Centralized Data Management Office website. Retrieved from http://cdmo.baruch.sc.edu/

Arango, C., Tank, J. L., Schaller, J. L., Royer, T. V., Bernot, M. J., & David, M. B. (2007). Benthic organic carbon influences denitrification in streams with high nitrate concentration. *Freshwater Biology*, *52*(7), 1210–1222. https://doi.org/10.1111/j.1365-2427.2007.01758.x

Beck, A. J., Kellum, A. A., Luek, J. L., & Cochran, M. A. (2016). Chemical flux associated with spatially and temporally variable submarine groundwater discharge, and chemical modification in the subterranean estuary at Gloucester Point, VA (USA). *Estuaries and Coasts*, *39*, 1–12. https://doi.org/10.1007/s12237-015-9972-0

Bilkovic, D. M., Mitchell, M. M., Davis, J., Herman, J., Andrews, E., King, A., et al. (2019). Defining boat wake impacts on shoreline stability toward management and policy solutions. *Ocean & Coastal Management*, *182*, 104945. https://doi.org/10.1016/j.ocecoaman.2019.104945

Boehm, A. B., Paytan, A., Shellenbarger, G. G., & Davis, K. A. (2006). Composition and flux of groundwater from a California beach aquifer: Implications for nutrient supply to the surf zone. *Continental Shelf Research*, *26*(2), 269–282. https://doi.org/10.1016/j.csr.2005.11.008

Bonin, P., & Raymond, N. (1990). Effects of oxygen on denitrification in marine sediments. *Hydrobiologia*, *207*(1), 115–122. https://doi.org/10.1007/BF00041447

Brandes, J. A., Devol, A. H., & Deutsch, C. (2007). New developments in the marine nitrogen cycle. *Chemical Reviews*, *107*(2), 577–589. https://doi.org/10.1002/chin.200720269

Burnett, W. C., Aggarwal, P. K., Aureli, A., Bokuniewicz, H., Cable, J. E., Charette, M. A., et al. (2006). Quantifying submarine groundwater discharge in the coastal zone via multiple methods. *Science of the Total Environment*, *367*(2–3), 498–543. https://doi.org/10.1021/acsami.6b16505

Cable, J. E., Corbett, D. R., & WalshMaud, M. (2002). Phosphate uptake in coastal limestone aquifers: A fresh look at wastewater management. *Limnology and Oceanography Bulletin*, *11*(2), 29–32. https://doi.org/10.1002/lob.200211229

Cai, W. J., & Sayles, F. L. (1996). Oxygen penetration depths and fluxes in marine sediments. *Marine Chemistry*, *52*(2), 123–131. https://doi.org/10.1016/0304-4203(95)00081-X

Charette, M. A., Allen, M. C., & Sites, F. (2006). Precision ground water sampling in coastal aquifers using a direct-push, shielded-screen well-point system materials and procedures. *Groundwater Monitoring & Remediation*, *26*(2), 87–93. https://doi.org/10.1111/j.1745-6592.2006.00076.x

Charette, M. A., & Buesseler, K. O. (2004). Submarine groundwater discharge of nutrients and copper to an urban subestuary of Chesapeake Bay (Elizabeth River). *Limnology and Oceanography*, *49*(2), 376–385. https://doi.org/10.4319/lo.2004.49.2.0376

Charette, M. A., & Sholkovitz, E. R. (2002). Oxidative precipitation of groundwater-derived ferrous iron in the subterranean estuary of a coastal bay. *Geophysical Research Letters*, *29*(10), 85-1–85-4. https://doi.org/10.1029/2001gl014512

Chesapeake Bay National Estuarine Research Reserve in Virginia. (2021). *Virginia Institute of marine science (CBNERR-VA VIMS)*. Virginia Estuarine and Coastal Observing System (VECOS). Retrieved from http://vecos.vims.edu

Cho, H. M., Kim, G., Kwon, E. Y., Moosdorf, N., Garcia-Orellana, J., & Santos, I. R. (2018). Radium tracing nutrient inputs through submarine groundwater discharge in the global ocean. *Scientific Reports*, *8*, 1–7. https://doi.org/10.1038/s41598-018-20806-2

Cornwell, J. C., Kemp, W. M., & Kana, T. M. (1999). Denitrification in coastal ecosystems: Methods, environmental controls, and ecosystem level controls, a review. *Aquatic Ecology*, *33*(1), 41–54. https://doi.org/10.1023/A:1009921414151

Correa, R. E., Tait, D. R., Sanders, C. J., Conrad, S. R., Harrison, D., Tucker, J. P., et al. (2020). Submarine groundwater discharge and associated nutrient and carbon inputs into Sydney Harbour (Australia). *Journal of Hydrology (Amsterdam)*, *580*, 124262. https://doi.org/10.1016/j.jhydrol.2019.124262

Domenico, P. A., & Schwartz, F. W. (1990). *Physical and chemical hydrology*. John Wiley & Sons.

Duque, C., Michael, H. A., & Wilson, A. M. (2020). The subterranean Estuary: Technical term, simple analogy, or source of confusion? *Water Resources Research*, *56*(2), 1–7. https://doi.org/10.1029/2019WR026554

Gruber, N., & Galloway, J. N. (2008). An Earth-system perspective of the global nitrogen cycle. https://doi.org/10.1038/nature06592

Guo, X., Xu, B., Burnett, W. C., Wei, Q., Nan, H., Zhao, S., et al. (2020). Does submarine groundwater discharge contribute to summer hypoxia in the Changjiang (Yangtze) River Estuary? *Science of the Total Environment*, *719*, 137450. https://doi.org/10.1016/j.scitotenv.2020.137450

Hall, W., Isla, R., Service, N. P., Park, A. N., Box, P. O., Harbor, B., et al. (2005). Denitrification capacity in a subterranean Estuary below a Rhode Island fringing salt marsh. *Estuaries*, *28*(6), 896–908. https://doi.org/10.1007/bf02696018

Hazen, A. XXIII. (1917). *Some physical properties of sands and gravels, with special reference to their use in filtration* (pp. 232–248). Harvard University Press. https://doi.org/10.4159/harvard.9780674600485.c25

Herbert, R. A. (1999). Nitrogen cycling in coastal marine ecosystems. *FEMS Microbiology Reviews*, *563–590*(5), 563–590. https://doi.org/10.1111/j.1574-6976.1999.tb00414.x

Hines, M. E., Knollmeyer, S. L., & Tugei, J. B. (1989). Sulfate reduction and other sedimentary biogeochemistry in a northern New England salt marsh. *Limnology and Oceanography*, *34*(3), 578–590. https://doi.org/10.4319/lo.1989.34.3.0578

Hvorslev, M. (1951). *Time lag and soil permeability in ground-water observations* (No. (36)). Waterways Experiment Station, Corps of Engineers, US Army.

Hwang, D.-W., Kim, G., Lee, W.-C., & Oh, H.-T. (2010). The role of submarine groundwater discharge (SGD) in nutrient budgets of Gamak Bay, a shellfish farming bay, in Korea. *Journal of Sea Research*, *64*(3), 224–230. https://doi.org/10.1016/j.seares.2010.02.006

Jiao, L., Wu, J., He, X., Wen, X., Li, Y., & Hong, Y. (2018). Significant microbial nitrogen loss from denitrification and anammox in the land-sea interface of low permeable sediments. *International Biodeterioration & Biodegradation*, *135*, 80–89. https://doi.org/10.1016/j.ibiod.2018.10.002

Killberg-Thoreson, L., Sipler, R. E., & Bronk, D. A. (2013). Anthropogenic nutrient sources supplied to a Chesapeake Bay tributary support algal growth: A bioassay and high-resolution mass spectrometry approach. *Estuaries and Coasts*, *36*(5), 966–980. https://doi.org/10.1007/s12237-013-9604-5

Kim, G., Kim, J. S., & Hwang, D. W. (2011). Submarine groundwater discharge from oceanic islands standing in oligotrophic oceans: Implications for global biological production and organic carbon fluxes. *Limnology and Oceanography*, *56*(2), 673–682. https://doi.org/10.4319/lo.2011.56.2.0673

Krest, J. M., Moore, W. S., Gardner, L. R., & Morris, J. T. (2000). Marsh nutrient export supplied by groundwater discharge: Evidence from radium measurements. *Global Biogeochemical Cycles*, *14*(1), 167–176. https://doi.org/10.1029/1999GB001197

Kroeger, K. D., & Charette, M. A. (2008). Nitrogen biogeochemistry of submarine groundwater discharge. *Limnology and Oceanography*, *53*(3), 1025–1039. https://doi.org/10.4319/lo.2008.53.3.1025

Kroeger, K. D., Swarzenski, P. W., Crusius, J., Bratton, J. F., & Charette, M. A. (2007). Submarine ground-water discharge: Nutrient loading and nitrogen transformations (No. (2006–3110)). US Geological Survey.

Lake, S. J., & Brush, M. J. (2015). Contribution of nutrient and organic matter sources to the development of periodic hypoxia in a tributary Estuary. *Estuaries and Coasts*, *38*(6), 2149–2171. https://doi.org/10.1007/s12237-015-9954-2

Leote, C., Iba, Æ. J. S., & Rocha, C. (2008). Submarine Groundwater Discharge as a nitrogen source to the Ria Formosa studied with seepage meters. *Biogeochemistry*, *88*(2), 185–194. https://doi.org/10.1007/s10533-008-9204-9

Lisa, J. A., Song, B., Tobias, C. R., & Duernberger, K. A. (2014). Impacts of freshwater flushing on anammox community structure and activities in the New River Estuary, USA. *Aquatic Microbial Ecology*, *72*(1), 17–31. https://doi.org/10.3354/ame01682

Luek, J. L., & Beck, A. J. (2014). Radium budget of the York River estuary (VA, USA) dominated by submarine groundwater discharge with a seasonally variable groundwater end-member. *Marine Chemistry*, *165*(55–65), 55–65. https://doi.org/10.1016/j.marchem.2014.08.001

McKenzie, T., Dulai, H., & Fuleky, P. (2021). Traditional and novel time-series approaches reveal submarine groundwater discharge dynamics under baseline and extreme event conditions. *Scientific Reports*, *11*(1), 22570. https://doi.org/10.1038/s41598-021-01920-0

Mitchell, M., Isdell, R. E., Herman, J., & Tombleson, C. (2021). Impact assessment and management challenges of key rural human health infrastructure under sea level rise. *Frontiers in Marine Science*, *8*, 631757. https://doi.org/10.3389/fmars.2021.631757

Moore, W. S. (1999). The subterranean estuary: A reaction zone of ground water and sea water. *Marine Chemistry*, *65*(1–2), 111–125. https://doi.org/10.1016/S0304-4203(99)00014-6

Moore, W. S. (2009). The effect of submarine groundwater discharge on the ocean. *Annual Review of Marine Science*, *2*(1), 59–88. https://doi.org/10.1146/annurev-marine-120308-081019

Mulholland, M. R., Morse, R. E., Boneillo, G. E., Bernhardt, P. W., Filippino, K. C., Procise, L. A., et al. (2009). Understanding causes and impacts of the dinoflagellate, cochlodinium polykrikoides, blooms in the Chesapeake Bay. *Estuaries and Coasts*, *32*(4), 734–747. https://doi.org/10.1007/s12237-009-9169-5

Nicholls, J. C., & Trimmer, M. (2009). Widespread occurrence of the anammox reaction in estuarine sediments. *Aquatic Microbial Ecology*, *55*, 105–113. https://doi.org/10.3354/ame01285

Nixon, S. W. (1995). Coastal marine eutrophication: A definition, social causes, and future concerns. *Ophelia*, *41*(1), 199–219. https://doi.org/10.1080/00785236.1995.10422044

O'Connor, A. E., Krask, J. L., Canuel, E. A., & Beck, A. J. (2018). Seasonality of major redox constituents in a shallow subterranean estuary. *Geochimica et Cosmochimica Acta*, *224*, 344–361. https://doi.org/10.1016/J.GCA.2017.10.013

O'Connor, A. E., Luek, J. L., Mcintosh, H., & Beck, A. J. (2015). Geochemistry of redox-sensitive trace elements in a shallow subterranean estuary. *Marine Chemistry*, *172*, 70–81. https://doi.org/10.1016/j.marchem.2015.03.001

Oh, J., & Silverstein, J. (1999). Oxygen inhibition of activated sludge denitrification. *Water Research*, *33*(8), 1925–1937. https://doi.org/10.1016/S0043-1354(98)00365-0

Oshiki, M., Satoh, H., & Okabe, S. (2016). Ecology and physiology of anaerobic ammonium oxidizing bacteria. *Environmental Microbiology*, *18*(9), 2784–2796. https://doi.org/10.1111/1462-2920.13134

Percuoco, V. P., Kalnejais, L. H., Officer, L. V., & Usa, N. H. (2015). Nutrient release from the sediments of the great Bay Estuary. *Estuarine, Coastal and Shelf Science*, *161*, 76–87. https://doi.org/10.1016/j.ecss.2015.04.006

Portnoy, J. W., Nowicki, B. L., Roman, C. T., & Urish, D. W. (1998). The discharge of nitrate-contaminated groundwater from developed shoreline to marsh-fringed estuary. *Water Resources Research*, *34*(11), 3095–3104. https://doi.org/10.1029/98WR02167

Reay, W. G. (2009). Water quality within the York River Estuary. *Journal of Coastal Research*, (10057), 23–39. https://doi.org/10.2112/1551-5036-57.sp1.23

Reay, W. G., Gallagher, D. L., & Simmons, G. M., Jr. (1992). Groundwater discharge and its impact on surface water quality in a Chesapeake Bay inlet. *JAWRA Journal of the American Water Resources Association*, *28*(6), 1121–1134. https://doi.org/10.1111/j.1752-1688.1992.tb04023.x

Robinson, C. E., Xin, P., Santos, I. R., Charette, M. A., Li, L., & Barry, D. A. (2018). Groundwater dynamics in subterranean estuaries of coastal unconfined aquifers: Controls on submarine groundwater discharge and chemical inputs to the ocean. *Advances in Water Resources*, *115*, 315–331. https://doi.org/10.1016/j.advwatres.2017.10.041

Rodellas, V., Stieglitz, T. C., Andrisoa, A., Cook, P. G., Raimbault, P., Tamborski, J. J., et al. (2018). Groundwater-driven nutrient inputs to coastal lagoons: The relevance of lagoon water recirculation as a conveyor of dissolved nutrients. *Science of the Total Environment*, *642*, 764–780. https://doi.org/10.1016/j.scitotenv.2018.06.095

Rosenberry, D. O., Labaugh, J. W., & Hunt, R. J. (2008). Use of monitoring wells, portable piezometers, and seepage meters to quantify flow between surface water and ground water. *Field Techniques for Estimating Water Fluxes Between Surface Water and Ground Water*, *4*, 39–70.

Ruiz-González, C., Rodellas, V., & Garcia-Orellana, J. (2021). The microbial dimension of submarine groundwater discharge: Current challenges and future directions. *FEMS Microbiology Reviews*, *45*(5), fuab010. https://doi.org/10.1093/femsre/fuab010

Sáenz, J. P., Hopmans, E. C., Rogers, D., Henderson, P. B., Charette, M. A., Schouten, S., et al. (2012). Distribution of anaerobic ammonia-oxidizing bacteria in a subterranean estuary. *Marine Chemistry*, *136–137*, 7–13. https://doi.org/10.1016/j.marchem.2012.04.004

Santoro, A. E., Francis, C. A., De Sieyes, N. R., & Boehm, A. B. (2008). Shifts in the relative abundance of ammonia-oxidizing bacteria and archaea across physicochemical gradients in a subterranean estuary. *Environmental Microbiology*, *10*(4), 1068–1079. https://doi.org/10.1111/j.1462-2920.2007.01547.x

Santos, I. R., Burnett, W. C., Dittmar, T., Suryaputra, I. G. N. A., & Chanton, J. (2009). Tidal pumping drives nutrient and dissolved organic matter dynamics in a Gulf of Mexico subterranean estuary. *Geochimica et Cosmochimica Acta*, *73*(5), 1325–1339. https://doi.org/10.1016/j.gca.2008.11.029

Santos, I. R., Chen, X., Lecher, A., Sawyer, A., Moosdorf, N., Rondellas, V., et al. (2021). Submarine groundwater discharge impacts on coastal nutrient biogeochemistry. *Nature Reviews Earth & Environment*, *108–119*(5), 307–323. https://doi.org/10.1016/B978-0-12-409548-9.11482-4

Schutte, C. A., Wilson, A. M., Evans, T., Moore, W. S., & Joye, S. B. (2017). Deep oxygen penetration drives nitrification in intertidal beach sands. *Limnology and Oceanography*, *63*(S1), 1–16. https://doi.org/10.1002/lno.10731

Scott, M. K., & Moran, S. B. (2001). Ground water input to coastal salt ponds of southern Rhode Island estimated using ^{226}Ra as a tracer. *Journal of Environmental Radioactivity*, *54*(1), 163–174. https://doi.org/10.1016/S0265-931X(00)00172-7

Seitzinger, S., Harrison, J. A., Böhlke, J. K., Bouwman, A. F., Lowrance, R., Peterson, B., et al. (2006). Denitrification across landscapes and waterscapes: A synthesis. *Ecological Applications*, *16*(6), 2064–2090. https://doi.org/10.1890/1051-0761(2006)016[2064:DALAWA]2.0.CO;2

Sin, Y., Wetzel, R. L., & Anderson, I. C. (1999). Spatial and temporal characteristics of nutrient and phytoplankton dynamics in the York River Estuary, Virginia: Analyses of long-term data. *Estuaries*, *22*(2), 260–275. https://doi.org/10.1007/BF02692120

Slomp, C. P., & Cappellen, P. V. (2004). Nutrient inputs to the coastal ocean through submarine groundwater discharge: Controls and potential impact. *Journal of Hydrology (Amsterdam)*, *295*(1–4), 64–86. https://doi.org/10.1016/j.jhydrol.2004.02.018

Smith, R. L., Böhlke, J. K., Song, B., & Tobias, C. R. (2015). Role of anaerobic ammonium oxidation (anammox) in nitrogen removal from a freshwater aquifer. *Environmental Science & Technology*, *49*(20), 12169–12177. https://doi.org/10.1021/acs.est.5b02488

Song, B., & Tobias, C. R. (2011). Methods in enzymology: Chapter 3 molecular and stable isotope methods to detect and measure anaerobic ammonium oxidation (ANAMMOX) in aquatic ecosystems (Vol. *63–89*).

Spiteri, C., Cappellen, P. V., & Regnier, P. (2008). Surface complexation effects on phosphate adsorption to ferric iron oxyhydroxides along pH and salinity gradients in estuaries and coastal aquifers. *Geochimica et Cosmochimica Acta*, *72*(14), 3431–3445. https://doi.org/10.1016/j.gca.2008.05.003

Spiteri, C., Slomp, C. P., Charette, M. A., Tuncay, K., & Meile, C. (2008). Flow and nutrient dynamics in a subterranean estuary (Waquoit Bay, MA, USA). *Field data and reactive transport modeling*, *72*(14), 3398–3412. https://doi.org/10.1016/j.gca.2008.04.027

Spiteri, C., Slomp, C. P., Tuncay, K., & Meile, C. (2008). Modeling biogeochemical processes in subterranean estuaries: Effect of flow dynamics and redox conditions on submarine groundwater discharge of nutrients. *Water Resources Research*, *44*(2), 1–18. https://doi.org/10.1029/2007WR006071

Stanley, B. C. (2021). *Differential nitrogen uptake by aquatic communities in a Chesapeake Bay tributary and in the coastal Alaskan Arctic*. The College of William & Mary, Virginia Institute of Marine Science.

Stewart, B. T., Bryan, K. R., Pilditch, C. A., & Santos, I. R. (2018). Submarine groundwater discharge estimates using radium isotopes and related nutrient inputs into Tauranga Harbour (New Zealand). *Estuaries and Coasts*, *41*(2), 384–403. https://doi.org/10.1007/s12237-017-0290-6

Talbot, J. M., Kroeger, K. D., Rago, A., Allen, M. C., & Charette, M. A. (2003). Nitrogen flux and speciation through the subterranean estuary of Waquoit Bay, Massachusetts. *The Biological Bulletin*, *205*(2), 244–245. https://doi.org/10.2307/1543276

Taniguchi, M., Burnett, W. C., Cable, J. E., & Turner, J. V. (2003). Assessment methodologies for submarine groundwater discharge. In M. Taniguchi, K. Wang, & T. Gamo (Eds.), *Land and marine hydrogeology* (pp. 1–23). Elsevier.

Tobias, C. R., Anderson, I. C., Canuel, E. A., & Macko, S. A. (2001). Nitrogen cycling through a fringing marsh-aquifer ecotone. *Marine Ecology Progress Series*, *210*, 25–39. https://doi.org/10.3354/meps210025

Valiela, I., Costa, J., Foreman, K., Teal, J. M., Howes, B., & Aubrey, D. (1990). Transport of groundwater-borne nutrients from watersheds and their effects on coastal waters. *Biogeochemistry*, *10*(3), 177–197. https://doi.org/10.1007/BF00003143

Wang, G., Han, A., Chen, L., Tan, E., & Lin, H. (2018). Fluxes of dissolved organic carbon and nutrients via submarine groundwater discharge into subtropical Sansha Bay, China. *Estuarine, Coastal and Shelf Science*, *207*, 269–282. https://doi.org/10.1016/j.ecss.2018.04.018

Wang, X., Du, J., Ji, T., Wen, T., Liu, S., & Zhang, J. (2014). An estimation of nutrient fluxes via submarine groundwater discharge into the Sanggou Bay-A typical multi-species culture ecosystem in China. *Marine Chemistry*, *167*, 113–122. https://doi.org/10.1016/j.marchem.2014.07.002

Wilson, S. (2022). The fate and transport of nitrogen in subterranean estuaries, (Dissertations, Theses, and Masters Projects). William & Mary. https://dx.doi.org/10.25773/v5-18sm-k126

Wong, W. W., Applegate, A., Poh, S. C., & Cook, P. L. M. (2020). Biogeochemical attenuation of nitrate in a sandy subterranean estuary: Insights from two stable isotope approaches. *Limnology and Oceanography*, *65*(12), 3098–3113. https://doi.org/10.1002/lno.11576

Woods, M. (2021). *Feedbacks among benthic metabolism, nitrogen cycling, and intense phytoplankton blooms in the York River Estuary*. The College of William & Mary.

Wu, J., Hong, Y., Wilson, S. J., & Song, B. (2021). Microbial nitrogen loss by coupled nitrification to denitrification and anammox in a permeable subterranean estuary at Gloucester Point, Virginia. *Marine Pollution Bulletin*, *168*, 112440. https://doi.org/10.1016/j.marpolbul.2021.112440

Zhang, Y., Santos, I. R., Li, H., Wang, Q., Xiao, K., Guo, H., & Wang, X. (2020). Submarine groundwater discharge drives coastal water quality and nutrient budgets at small and large scales. *Geochimica et Cosmochimica Acta*, *290*, 201–215. https://doi.org/10.1016/j.gca.2020.08.026